Received: November 16, 2024. Revised: December 17, 2024.

International Journal of
Intelligent Engineering & Systems

http://www.inass.org/

Optimizing Permanent Magnet Synchronous Motor Performance Considering Both Maximum Torque Per Ampere and Field Weakening

Cao Ngoc Dien[1] Huynh Hoang Bao Nghia[1] Le Cao Quyen[1] Le Van Dai[1]*

[1]*Faculty of Electrical Engineering Technology, Industrial University of Ho Chi Minh City, Ho Chi Minh City, Vietnam*
Corresponding author's Email: levandai@iuh.edu.vn

Abstract: This paper proposes a novel control structure for permanent magnet synchronous motors (PMSMs), integrating a fuzzy logic-enhanced PI controller (FPI) with maximum torque per ampere (MTPA) and field weakening (FW) strategies. The primary objective is to address the nonlinear behavior of PMSMs, particularly the complex relationship between reference speed and torque, while simultaneously minimizing copper losses, total harmonic distortion (THD), and thermal losses. The FPI controller enhances the performance of traditional PI control by dynamically adjusting parameters, improving control accuracy under nonlinear conditions, and mitigating cross-coupling effects between the *d*- and *q*-axis. The combination of MTPA and FW allows the motor to achieve optimal efficiency at both low and high speeds. At the same time, FPI is crucial in improving control quality, reducing THD, and minimizing energy losses. Compared to advanced control methods such as artificial neural networks (ANN) or model predictive control (MPC), the FPI controller provides a practical, resource-efficient solution. Its simplicity and lower computational demand make it ideal for real-time applications, while still delivering robust performance. Simulation results using MATLAB/Simulink with a salient-pole PMSM demonstrate the effectiveness of the proposed approach. The FPI controller outperforms the traditional PI controller in reducing %THD, with a reduction of 8.96% in MTPA mode (PI: 146.12%, FPI: 137.16%) and 61.26% in MTPA-FW mode (PI: 709.03%, FPI: 647.77%). Furthermore, the FPI controller increases motor efficiency by 0.35% in MTPA mode and 0.26% in MTPA-FW mode. These improvements contribute to better current waveform quality, reduced energy losses, and thermal losses, thus extending the lifespan of components and enhancing system stability. The findings underscore the FPI controller's capability to optimize PMSM performance, particularly in applications demanding high energy efficiency, power stability, and precision speed control. The results show that the FPI controller combined with the MTPA-FW strategy provides a high-performance, reliable solution for PMSM systems. Furthermore, these findings indicate that the MTPA-FW strategy has strong potential in applications such as electric vehicles, crewless aerial vehicles, and systems requiring precise control at high speeds, opening up promising research and development directions for the future.

Keywords: Permanent magnet synchronous motor (PMSM), Maximum torque per ampere (MTPA), Field weakening (FW), Fuzzy-based PI controller (FPI), Total harmonic distortion (THD), Speed and torque control.

1. Introduction

PMSM offers high efficiency, power density, and reliability, making it widely used in electric vehicles, rail transport, and industrial applications [1]. Advances in permanent magnet materials have enhanced their suitability for high-performance uses [2, 3]. Salient pole PMSMs are favored in hybrid and electric vehicles due to their high torque density and capability to maintain constant power over a broad speed range [4, 5]. This type of motor generates torque from permanent magnet flux and reluctance torque due to non-uniform air gaps, which result in different *d*- and *q*-axis inductances [6, 7]. These features support FW operation [8, 9], but the non-uniform inductances cause cross-magnetization between *d*- and *q*-axis currents and magnetic saturation, making the motor a nonlinear system [10, 11]. Furthermore, the flux intensity from the

permanent magnets depends on the motor's operating temperature. During operation, internal parameter variations and external disturbances impact the motor's performance [7, 12]. Given the characteristics, controlling the speed of salient pole PMSMs presents a challenge that has been the subject of research for many years.

Previous studies on PMSM control methods have shown strengths and limitations. Research [13] employs direct torque, fractional-order, and sliding mode control to enhance stability and flexibility at high speeds. Experimental results show that this method increases torque performance by 15% at high speeds compared to traditional control methods. However, this approach adds computational complexity and requires robust hardware, making its implementation more challenging. According to research [14] field-oriented control (FOC) maintains the *d*-axis current at zero to optimize performance at low and medium speeds. In practical tests, this method shows stable performance below 3000 rpm; however, it struggles to maintain efficiency at higher speeds when the motor faces rapid speed changes, leading to unstable performance. Another study [15] focuses on reducing cross-coupling between the *d*- and *q*-axis currents to increase accuracy but lacks speed range flexibility, limiting its applicability in systems requiring high speeds. Specifically, this study achieved 95% accuracy in reducing cross-coupling, but the operating speed range remains limited to 2500 rpm. Research [16] shows that applying a current limit circle in deep FW modes helps stabilize the *q*-axis current and improves control efficiency, reducing current fluctuations by 12% at high speeds.

On the other hand, the MTPA method combined with FW allows for the regulation of both the *d*- and *q*-axes currents, thus expanding the motor's speed range without reducing torque. Practical tests on PMSM motor systems using MTPA and FW show an 18% improvement in performance at high speeds compared to other control methods. This helps enhance efficiency in applications such as electric vehicles, especially when a quick load response is needed. However, using FW can reduce control efficiency at high speeds due to interference from the *q*-axis current, leading to a 10% increase in energy loss in deep FW modes [7]. Fuzzy logic methods have significant advantages for power systems and electric drive applications [17, 18]. However, again, the study does not provide specific data or results to demonstrate how fuzzy logic improves control performance in this study. For these reasons, this study proposes an FPI controller to enhance the PMSM drive performance, addressing the slow response of traditional PI controllers. Although there are extensive studies on optimizing PI parameters, challenges such as convergence and fast identification remain.

The proposed method enhances the speed range of PMSMs by integrating MTPA control for low and medium speeds with FW for high speeds. The FPI controller optimizes the coefficients of the conventional PI controller, resulting in improved stability and response. Simulations demonstrate that the FPI controller enhances the reference speed tracking capability and overall system performance in PMSM drives. This study makes several contributions as follows: (***i***) Improving the control quality by identifying the PI coefficient, (***ii***) Extending the speed operating range beyond the rated speed, and (***iii***) Developing an FPI controller along with fuzzy control rules and speed signal fuzzification and defuzzification. Therefore, this paper presents and implements a control technique based on the structure of the FOC controller to combine the MTPA and MTPA-FW control strategies to compare the dynamic response based on the FPI controller and the traditional PI controller through MATLAB/Simulink. The structure of the paper is as follows: Section 2 presents the theoretical basis and model of the PMSM, Section 3 outlines the control strategy, and Section 4 presents the simulation results.

2. Theory foundation

2.1 PMSM model

The PMSM model in the *dq* reference frame uses space vector theory. A coordinate transformation reduces the voltage equations from three variables (*abc*) to two (*dq*), aligning the *dq* frame with the rotor at the stator's synchronous speed ω_e. This results in simplified stator voltage equations [19, 20]:

$$\begin{cases} u_d = R_s i_d - \omega_e L_q i_q \\ u_q = R_s i_q + \omega_e (\varphi_m + L_d i_d) \end{cases} \quad (1)$$

where u_d and u_q are the *d*- and *q*-axis stator voltages, respectively; i_d and i_q are the *d*- and *q*-axis stator currents, respectively; R_s is the stator resistance; ω_e is the synchronous electrical speed, φ_m is the permanent magnet flux linkage and L_d, and L_q are the *d*- and *q*-axis inductances, respectively. Therefore, the electromagnetic torque is produced as follows [8, 21]:

$$T_e = \frac{3}{2} p \varphi_m i_q + \frac{3}{2} p \left(L_d - L_q\right) i_d i_q \quad (2)$$

in which p is the number of pole pairs.

2.2 Current and voltage limit

In practical drive systems, PMSMs are powered by converters that convert AC/DC power into variable-frequency, variable-voltage three-phase AC for control. However, inverters have maximum voltage and current output limits, necessitating that the PMSM operates within a current limit (i_{s_max}) to avoid overheating and damage. Therefore, the current must satisfy specific conditions to ensure the safe operation of both the motor and the inverter. This approach is crucial for maintaining the integrity and longevity of the system components [1, 16, 22]:

$$i_s = \sqrt{i_d^2 + i_q^2} \le i_{s\_max} \tag{3}$$

Besides, neglecting the voltage drop across the resistance R_s, and i_s is the maximum-phase current respectively. The stater voltage is described as follows:

$$u_s = \sqrt{u_d^2 + u_q^2} \le u_{s\_max} \tag{4}$$

where $u_{s\_max} = u_{dc}/\sqrt{3}$ with u_{dc} being the DC link voltage. To ensure stable operation of the PMSM control system at high speeds without exceeding the maximum voltage limit u_{s_max}, constraints on d- and q-axis currents and d- and q-axis voltages must be applied. Considering the influence of rotor flux through the virtual current source i_f helps optimize the FW control strategy, ensuring that the motor flux is adjusted accordingly. This approach ensures that the total voltage does not exceed u_s, enhancing the system's efficiency. These constraints are applied by substituting Eq. (1) into Eq. (4), resulting in [12, 22]:

$$1 \ge \frac{u_{s\_max}^2}{\frac{u_{s\_max}^2}{(\omega_e L_q)^2}} + \frac{(i_d + i_f)^2}{\frac{u_{s\_max}^2}{(\omega_e L_d)^2}} \tag{5}$$

From Eq. (5), it can be seen that the voltage limit region takes the form of an ellipse, centered at ($-i_f$, 0) with the semi-major axeis as $\frac{u_{s\_max}}{\omega_e L_d}$ and semi-minor axis as $\frac{u_{s\_max}}{\omega_e L_q}$, as shown in Fig. 1 (a), for the PMSM with infinite constant power speed range (CPSR) the optimal current trajectory that achieves the maximum output torque can be divided into three regions [23]. Considering curve OA, the motor operates in constant torque mode, and the ideal current trajectory follows the MTPA curves to achieve MTPA. The FW control is not required since current and voltage constraints limit the operating region.

Considering curve AB, the motor operates at the intersection of the voltage and current limit boundaries, corresponding to curve AB. Within the region OABCO, the trajectory is constrained by the voltage limit circle but remains within the current limit circle. FW control is necessary to ensure the total system stays within allowable limits, maintaining performance stability. The integration of MTPA and FW control is discussed in the following section

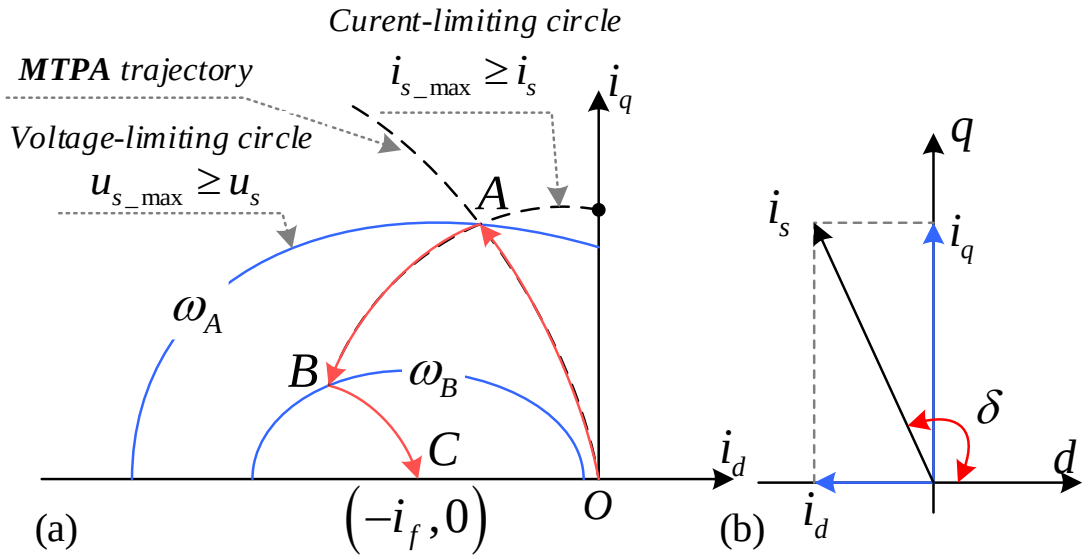

Figure. 1 Graph: (a) Operation regions with infinite CPSR ($\omega_A < \omega_B$) and (b) The angle of the developed torque

2.3 Maximum torque per ampere method

The MTPA method optimizes the stator current vector to minimize the *d*- and *q*-axis current components while producing the required torque. As shown in Fig. 1 (b), this method effectively reduces copper loss, which constitutes about 80% of total motor losses at low speeds, by maximizing torque for a given current magnitude or minimizing current for a specified torque. [13, 24]. From Fig. 1 (b), the *d*- and *q*-axis stator currents can be deduced as follows:

$$\begin{cases} i_d = i_s\, cos(\delta) \\ i_q = i_s\, sin(\delta) \end{cases} ; \quad 0 \le \delta \le 180° \tag{6}$$

where δ and i_s are the torque angle and stator current vectors, respectively. We can rewrite the torque equation as follows by substituting Eq. (6) into Eq. (2). Because $sin\,\delta\, cos\,\delta = \frac{1}{2} sin\, 2\delta$, can be rewritten as.

$$T_e = \frac{3}{2} p \begin{bmatrix} \varphi_m (i_s\, sin\,\delta) \\ +\frac{1}{2}\left(L_d - L_q\right)(i_s^2\, sin\, 2\delta) \end{bmatrix} \tag{7}$$

Therefore, the reluctance torque (T_r) and excitation torque of the magnet (T_m) can be expressed from Eq. (7) as:

$$T_e = \underbrace{\frac{3}{2} p \varphi_m (i_s\, sin\,\delta)}_{T_m} + \underbrace{\frac{3}{4}\left(L_d - L_q\right)(i_s^2\, sin\, 2\delta)}_{T_r} \tag{7}$$

The interior PMSM torque reaches its maximum at a torque angle that sets the derivative of the torque in Eq. (7) to zero. This angle can be derived as follows [25].

$$\varphi_m (i_s\, cos\,\delta) + (i_s\, cos\,\delta)^2 - (i_s\, cos\,\delta)^2 \left(L_d - L_q\right) = 0 \tag{8}$$

From Eq. (3), two solutions of i_d that the maximum the developed torque as a function of i_s are derived as follows:

$$i_d = \begin{cases} \frac{\varphi_m + \sqrt{\varphi_m^2 + 8\left(L_d - L_q\right)^2 i_s^2}}{4\left(L_d - L_q\right)} < 0 \\ \frac{\varphi_m - \sqrt{\varphi_m^2 + 8\left(L_d - L_q\right)^2 i_s^2}}{4\left(L_d - L_q\right)} > 0 \end{cases} \tag{9}$$

The flux linkage and inductance difference set the conditions; this difference indicates the saliency of the motor. For a non-salient motor, $L_d = L_q$, so the term (L_d - L_q) would be zero, making this expression undefined. This formula, therefore, applies to salient pole PMSMs, where $L_d \neq L_q$.

Boundary Condition 1: This occurs when the sum $\varphi_m + \sqrt{\varphi_m^2 + 8\left(L_d - L_q\right)^2 i_s^2}$ is negative. It specifies a situation where the flux linkage φ_m and the stator current interact in a way that keeps i_d positive or within a range that ensures stable operation.

Boundary Condition 2: This occurs when the difference $\varphi_m - \sqrt{\varphi_m^2 + 8\left(L_d - L_q\right)^2 i_s^2}$ positive. It provides another region for i_d Depending on the control strategy, achieve the desired FW or torque-producing component.

Since $L_d < L_q$ the torque angle should be larger than 90°. Therefore, the current i_d has a negative magnitude on the *d*-axis. Thus, the torque angle and stator current of the *d*- and *q*-axis that produces maximum torque can be derived as follows:

$$i_{d\_MTPA} = \frac{\varphi_m - \sqrt{\varphi_m^2 + 8\left(L_d - L_q\right)^2 \left|i_{s\_MTPA}^2\right|}}{4\left(L_d - L_q\right)} \tag{11}$$

$$i_{q\_MTPA} = \sqrt{\left|i_{s\_MTPA}^2\right| - i_{d\_MTPA}^2} \tag{12}$$

$$\delta_{MTPA} = tan^{-1}\left(\frac{i_{q\_MTPA}}{i_{d\_MTPA}}\right) \tag{13}$$

where i_{d_MTPA}, i_{q_MTPA}, and δ_{MTPA} are the stator currents for the *d*- and *q*-axis and the torque angle for the MTPA operating point. It is clear from Eqs. (7) to (13) that the supply current limits the maximum torque. Therefore, the voltage limitation was not considered in the constant-torque region.

2.4 Magnetic field weakening method

When using the FOC method to operate the motor at rated flux, the stator voltage, rated current, and back electromotive force limit the maximum speed. This speed is referred to as the rated speed. When exceeding this speed, the motor's operation becomes more complex because the back electromotive force surpasses the supply voltage. However, setting the *d*-axis stator current to a negative value reduces the rotor flux, allowing the motor to operate higher than the rated speed. This operation is known as FW control [12]. The MTPA control strategy is no longer

appropriate at higher speeds, and FW control should be considered. The *d*-axis current must be controlled so it weakens the stator flux linkage. Per-unit current components can be calculated using a maximum voltage u_{s_max} constraint [26]. The FW current components are as follows.

$$i_{d\_FW} = \frac{L_d\varphi_m - \sqrt{AB}}{(L_d^2 - L_q^2)} \tag{14}$$

$$i_{q\_FW} = \sqrt{\left|i_{s\_FW}^2\right| - i_{d\_FW}^2} \tag{15}$$

with $A = (L_d\varphi_m) + \left(L_d^2 - L_q^2\right)$ and $B = \left(\varphi_m^2 + L_q^2 i_{s\_FW}^2 - \frac{u_{s\_max}^2}{\omega_e^2}\right)$. These equations can be used to derive the current component values at various speeds and current levels of i_{d_FW}.

3. PMSM controller

3.1 Problem description

The PMSM control system design should address the following;

Remark 1: Under variable load conditions, FPI controller parameters may shift, but its self-adjusting capability allows the system to adapt, maintaining motor stability and efficiency.

Remark 2: During sudden load changes or power supply faults, the combined MTPA, FW, and FPI strategies help mitigate speed or torque fluctuations. MTPA optimizes torque per current, while FW extends the speed range, ensuring system stability despite unexpected disruptions.

3.2 The PI controller

The PMSM motor drive system Fig. 2 includes a speed controller, MTPA with FW, SV-PWM, and an inverter to enhance stability. Motor speed relies on stator current frequency and pole count, not the 50 Hz grid. As the load increases, a feedback control system with a speed sensor adjusts frequency and torque to maintain stable operation [13, 27].

The controller's primary function is to maintain the output at the desired level by minimizing the difference between the measured output and the reference value [28]. The transfer function of the PI controller model, as shown in Fig. 3, is shown as:

$$G_{PI}(s) = \frac{\Delta i(s)}{\Delta\omega(s)} = k_P + \frac{k_I}{s} - B_a \tag{16}$$

This study determines the PI controller coefficients using the Ziegler-Nichols ultimate frequency method. The proportional gain k_p is increased until the system oscillates persistently at the ultimate gain β. The feedback gain B_a and integral time constant k_i help generate proportional and adjustment signals to minimize error. The optimized PI coefficients are presented in Table 1, corresponding to Eq. (16).

$$G_{PI}(s) = 0.15689 + \frac{8.9938}{s} - 0.015 \tag{17}$$

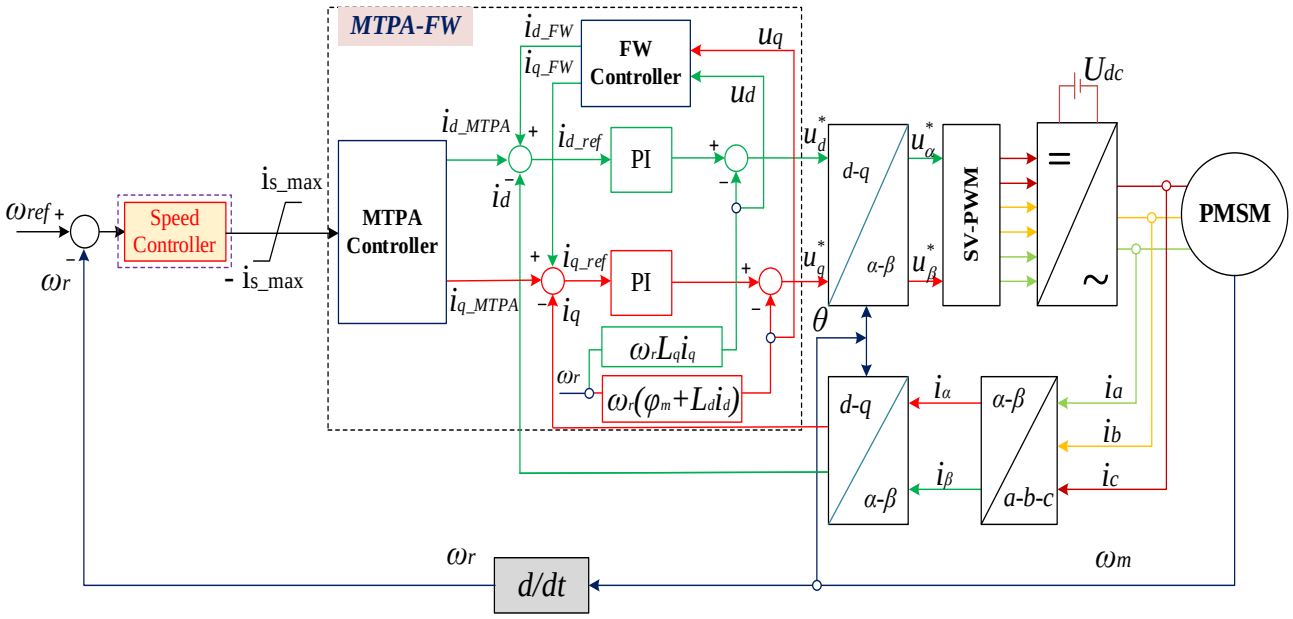

Figure. 2 PMSM control diagram

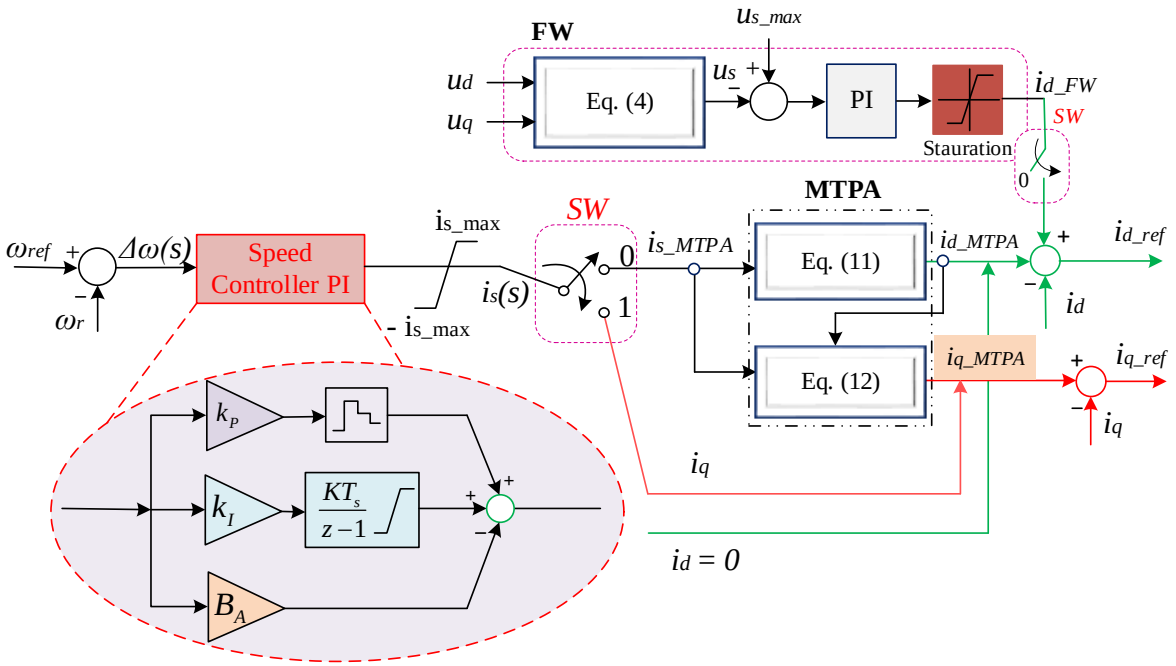

Figure. 3 MTPA and FW systems with PI controller according to transfer function model.

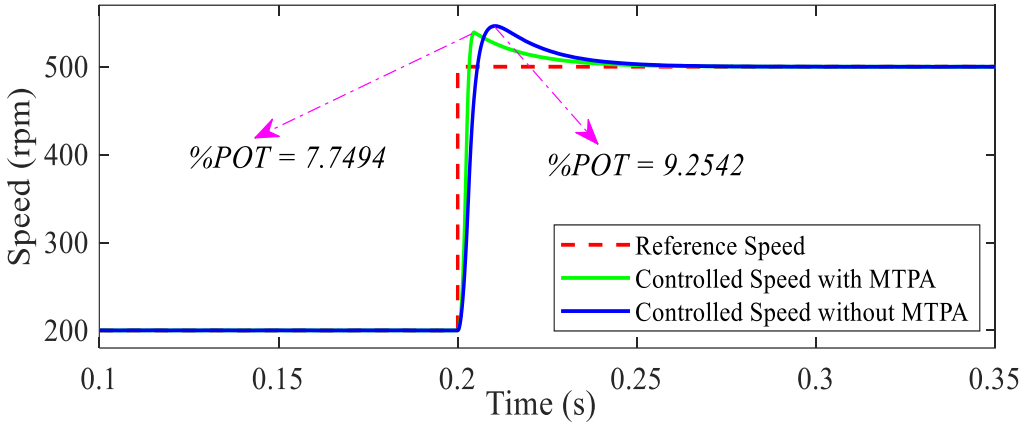

Figure. 4 The terminal speed response of the PMSM system with the PI controller

In a traditional PI controller, speed response using the MTPA method, as shown in Fig. 4, reaches the target speed faster and provides faster acceleration capability. Without MTPA, the motor experiences a delay of 0.2 sec when accelerating to 500 rpm, resulting in a slower response and longer processing time. The overshoot without MTPA is 9.2542, while with MTPA, the overshoot is reduced to 7.7494. This demonstrates that the MTPA method is well-suited to the control objectives for low-speed operation. However, the primary goal of this paper is to expand the operating range beyond the rated limits for PMSM motors. To address this, a new technique combining the MTPA method with FW and the proposed controller is applied, effectively resolving this issue, as discussed in Section 3.3.

Table 1. The parameter value of the PI controller

Para meter	k_P	k_I	B_a
Value	$\frac{5}{1827}\beta$	$\beta^2 k_P$	$\frac{2737\times10^{-6}\beta - 73\times10^{-4}}{10}$

3.3 The proposed controller

The objective is to design a controller capable of self-adjusting control parameters in the simplest way possible without requiring complex algorithms. Advanced controllers, such as Artificial Neural Networks, Model Predictive Control, and Deep Learning, can optimize performance but necessitate complex structures and powerful hardware, which increase costs and pose deployment challenges.

Hence, the FPI controller, with its simple structure, is easy to implement and does not demand high hardware configurations. Its outstanding advantages are demonstrated in the following design. As discussed in subsection 3.1, a traditional PI controller lacks high efficiency for PMSM control due to its fixed control signals. To address this, a fuzzy-based optimization method is introduced to adjust the PI coefficients, creating a hybrid control system shown in Fig. 5 that combines PI and fuzzy logic. The control signal from the MTPA and FW strategy in Eq. (16) is simplified by omitting B_a [24, 29, 30].

$$n_f(s) = \left[k_{P0}\Delta\omega(s) + k_{Pf}\right] + \left[k_{I0}\int_0^s \Delta\omega(s)ds + k_{If}\right] \quad (18)$$

in which k_{P0} and k_{I0} are the original coefficients of the PI controller. The k_{Pf} and k_{If} are the coefficients generated by the fuzzy to add the PI coefficients. The digital FPI controller is characterized by two input signals derived from the error $\Delta\omega$, and the control equation represents the output signal.

$$\Delta\omega(s) = \omega_{ref}(s) - \omega_r(s) \quad (19)$$

$$d\Delta\omega(s) = \Delta\omega(s) - \Delta\omega(s-1) \quad (20)$$

in which $\omega_{ref}(s)$ and $\omega_r(s)$ are the reference signal and the actual signal of the system, respectively; $\Delta\omega(s)$ and $d\Delta\omega(s)$ are the input functions to the FPI controller.

Step 1: Fuzzification: The fuzzification module converts the error $\omega_{ref}(s)$ and its change $\omega_r(s)$ into fuzzy values within the range [-10, 10]. The fuzzy subsets for $\omega_{ref}(s)$ are [NE, NSS, NS, ZE, PS, PSS, PO], and for $\omega_r(s)$, they are [NS, ZE, PS] [18, 28, 31].

Step 2: Fuzzy Control Rules: Fuzzy rules link input and output values. Subsets for k_{Pf} and k_{If} include [NEE, NE, NSS, NS, ZE, PS, PSS, PO, POO] and are defined from 0 to 1, as per If $(\Delta\omega)_1$ is $A_1^i \ldots$ and $(\Delta\omega)_n$ is A_n^i then $n_f = B^i$. Using 21 If-then rules, the system determines k_{Pf} and k_{If} based on $\omega_{ref}(s)$ and $\omega_r(s)$ inputs within a range of [-1, 1] shown in Fig. 6.

Step 3: Defuzzification: The defuzzification applies to converting the fuzzy value into numeric values. After the defuzzification, the two control coefficients, n_{fP} and n_{fI}, can be obtained from the proposed FPI strategy [29, 31, 32].

Table 2. The parameter value of the FPI controller

Parameter	k_{P0}	k_{I0}	k_{Pf}	k_{If}
Value	$\frac{5}{1827}\beta$	$\beta^2 k_P$	[-1 1]	[-1 1]

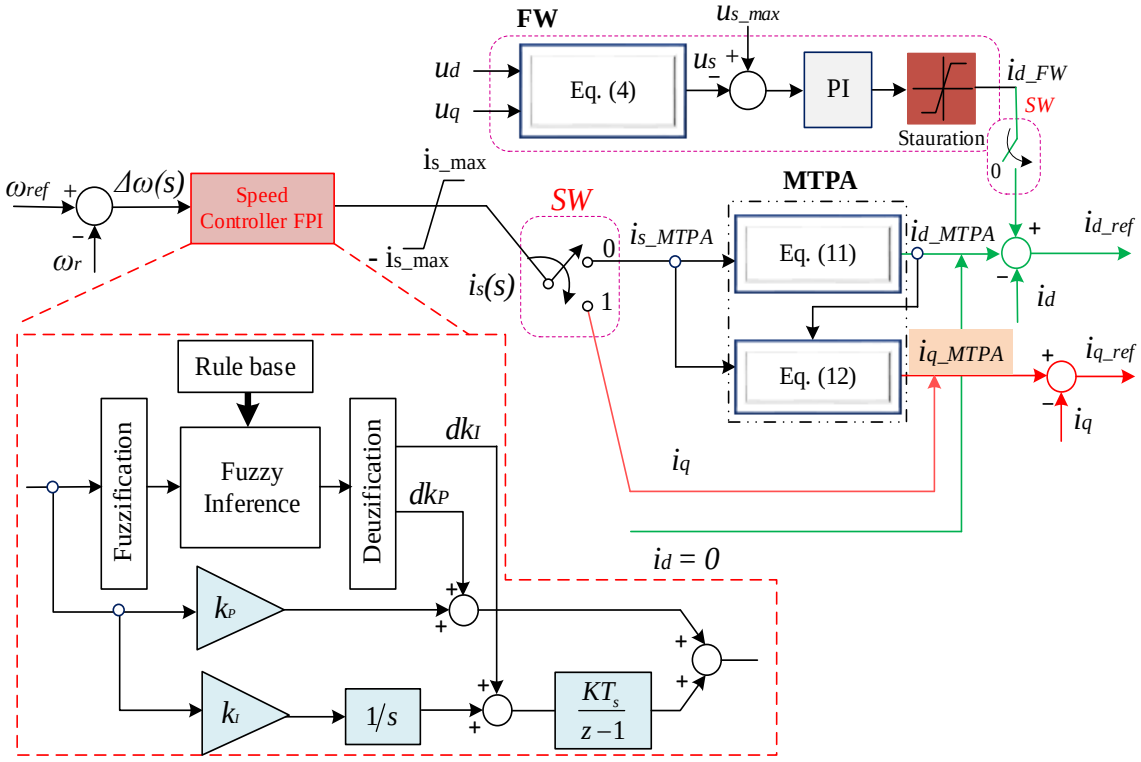

Figure. 5 MTPA and FW systems with FPI controller according to transfer function model

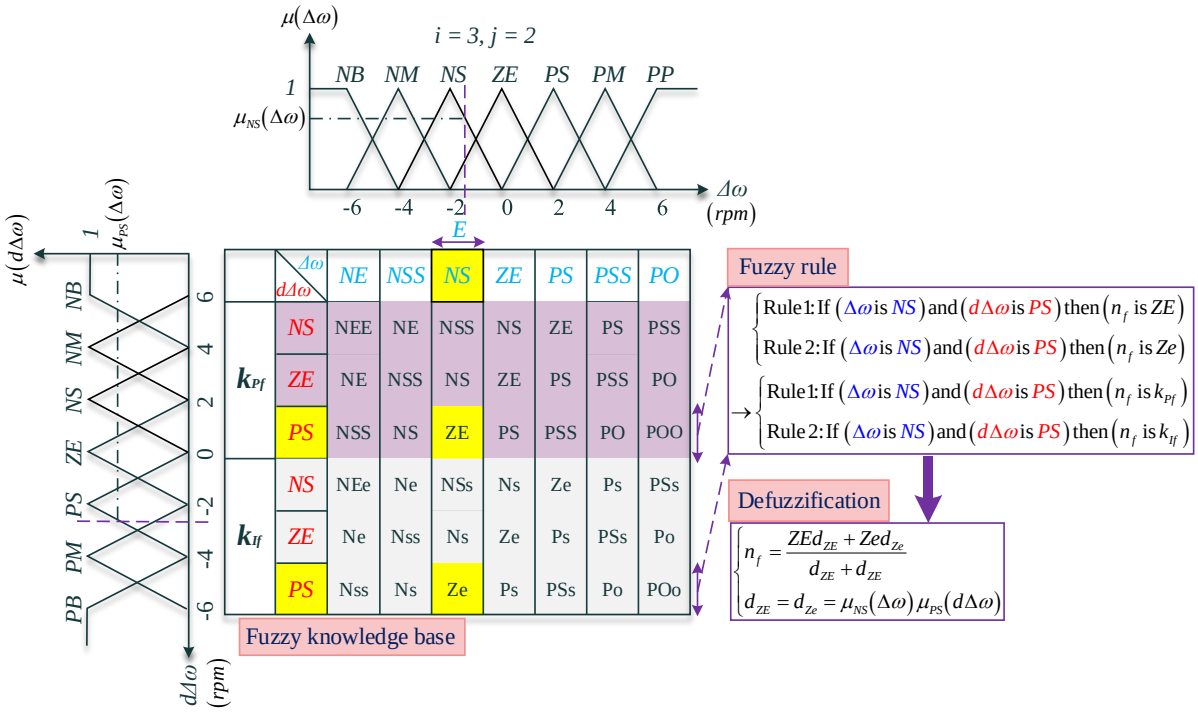

Figure. 6 The FPI controller for PMSM motors

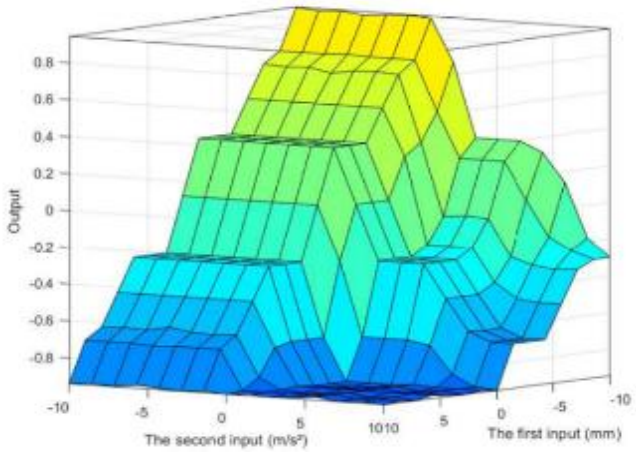

(a)

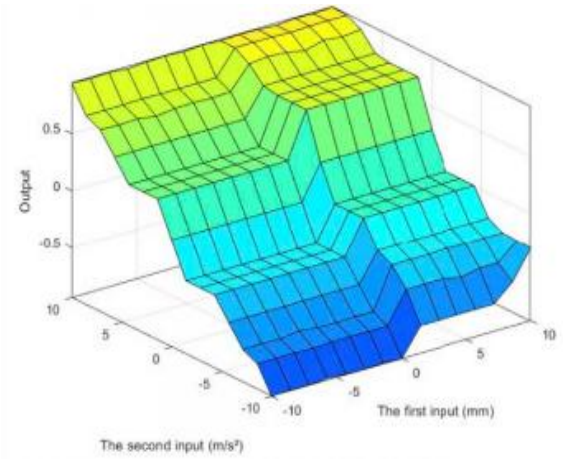

(b)

Figure. 7 Fuzzy surface: (a) Fuzzy surface (k_{Pf} coefficient) and (b) Fuzzy surface (k_{If} coefficient)

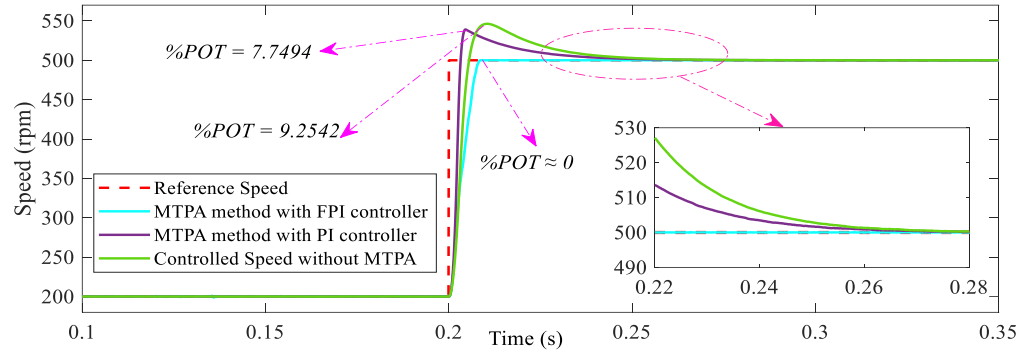

(a)

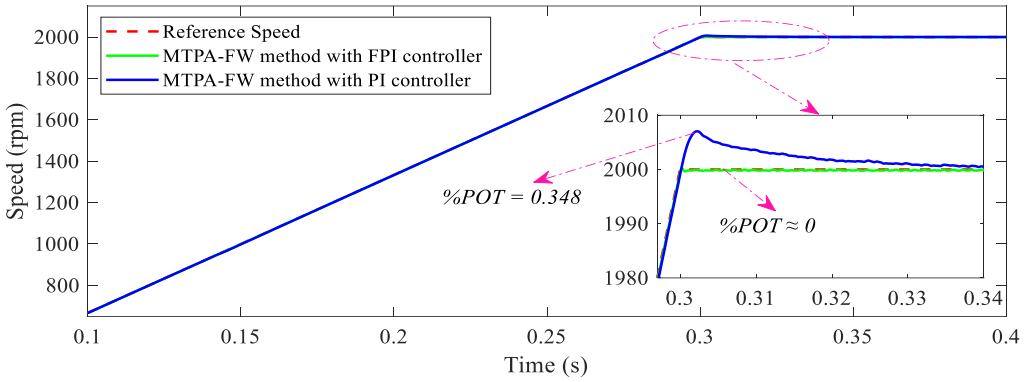

(b)

Figure. 8 The terminal speed response of the PMSM system with the FPI controller: (a) Speed response using the MTPA method and (b) Speed response using the MTPA-FW method

The fuzzy rules of the FPI controller are presented in Figs. (6) and (7), while the speed response at the final stage when the motor operates in MTPA mode is illustrated in Figs 8 (a) and (b). When the proposed method is applied with control parameters as specified in Table 2, the speed response quickly recovers to the setpoint, and the overshoot is nearly zero at 0.2 sec when the speed increases from 200 to 500 rpm. The other two methods exhibit significantly higher overshoot, as shown in Fig. 8 (a). When the motor operates in MTPA-FW mode, the proposed controller achieves zero overshoot again, whereas the PI controller records an overshoot of 0.348%. This demonstrates that the proposed controller is well-suited for PMSM motor speed control, ensuring stable operation, improved efficiency, and safe, effective performance under overspeed conditions.

4. Verification and analysis

The PMSM motor's speed control is modeled and simulated in MATLAB/Simulink, creating comparison frameworks to evaluate the proposed control structure's effectiveness. The analysis reveals that the proposed controller offers robust, stable responses under uncertain parameters and load disturbances, with improved dynamic reaction speed and accuracy [17, 33]. The simulation model is illustrated in Fig. 9, with the PMSM parameters provided in Table 3. In the simulation of PMSM control using the FPI controller combined with the MTPA and FW methods, the parameters are set as follows: the DC voltage supplied to the rectifier is U_{dc} = 311 V, the switching frequency is T_s = 10 µs, and the simulation time is t = 0.4 sec. The simulation, conducted using Matlab/Simulink, aims to evaluate the performance of the FPI controller in controlling PMSM speed compared to a conventional PI controller. Simulation cases are presented and compared based on numerical studies [34]:

Table 3. PMSM parameter

Parameter	Value	Parameter	Value
Rated Power P_r (kW)	3	Inductance in d-axis L_d (mH)	5.25
Rated speed n_r (rpm)	1200	Inductance in q-axis L_q (mH)	12
Number of pole pairs	4	Disc friction coefficient B (N.m.s)	0.008
Stator resistance R_s (Ω)	0.958	Flux linkage φ_m (Wb)	0.1827
Rotor and load inertia J (kg.m^2)	0.003		

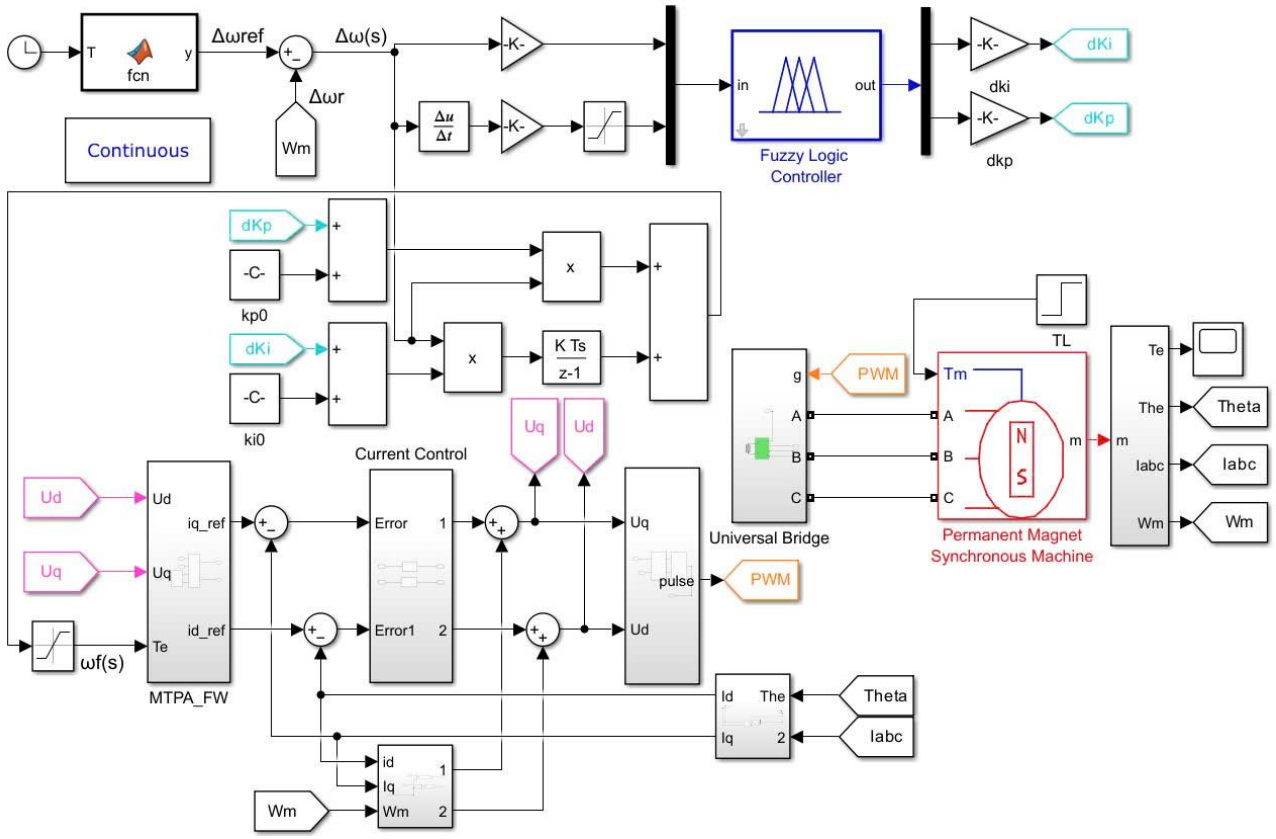

Figure. 9 The PMSM engine simulation model is tested

4.1 Speed changes suddenly and operates in MTPA mode

The motor operates at a base speed of 1000 rpm and is increased to 1200 rpm after approximately 0.2 sec, as shown in Fig. 10. The speed control loop effectively tracks the reference speed and compensates for load disturbances. However, the PI controller exhibits overshoot and oscillation before stabilizing, indicating poorer performance than the more stable FPI controller, which responds faster and without oscillation. Figs. 11 (b), (c), and (d) show that the FPI controller also has a quicker torque response than the PI controller. The motor operates at rated flux, with maximum speed limited by stator voltage, rated current, and back EMF, referred to as the rated speed. Exceeding this speed complicates operation, so this study combines the FW and MTPA methods to extend the PMSM motor's operating range beyond its rated speed, as discussed in case 4.2.

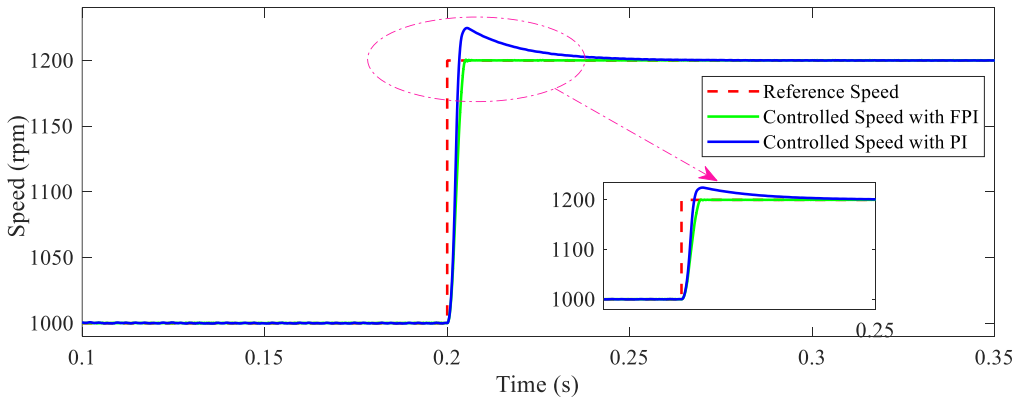

(a)

Figure. 10 (*cont.*)

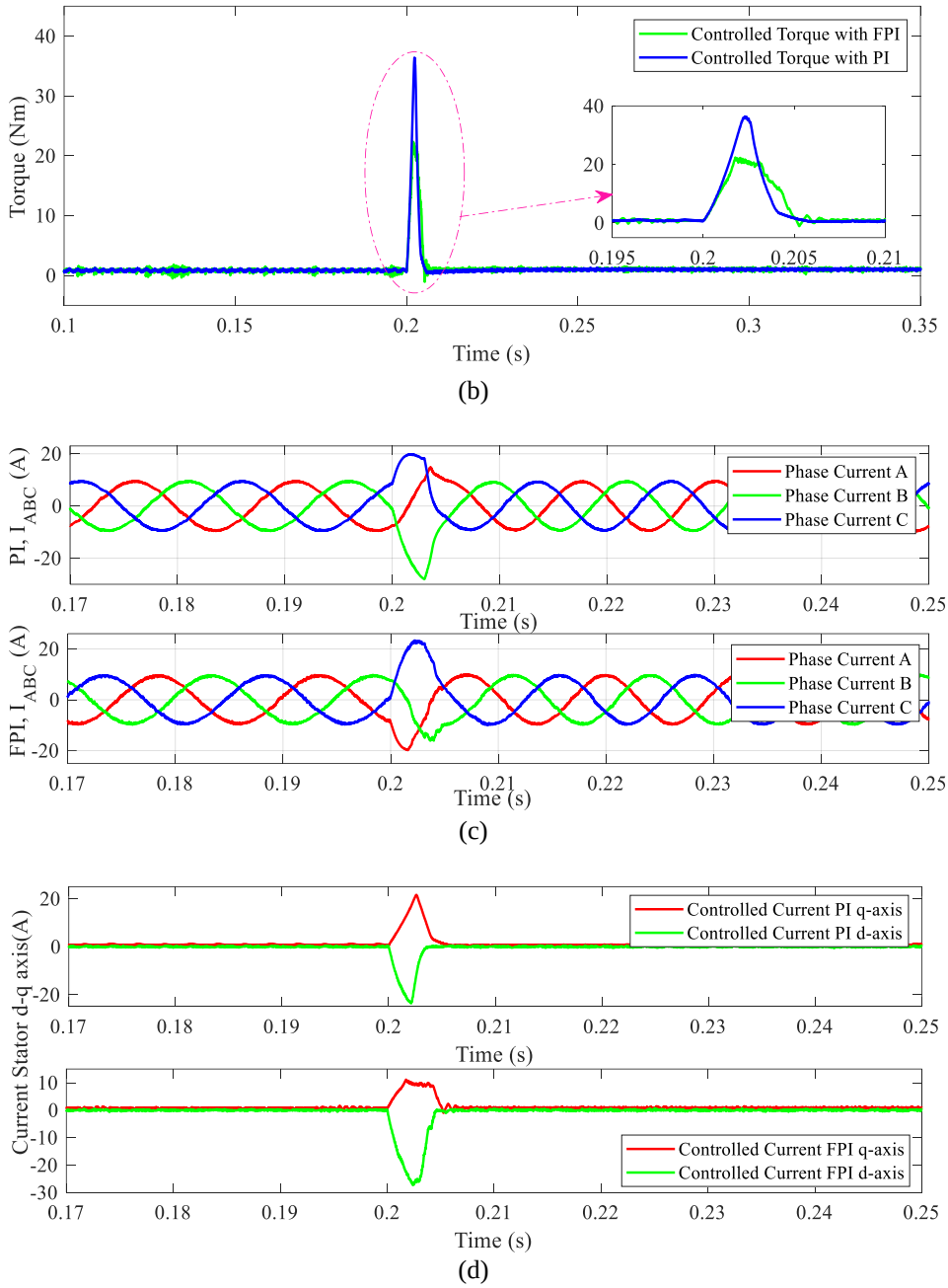

Figure. 10 PMSM control by MTPA when set speed ω_{ref} = [1000 1200] (rpm): (a) Speed response of the PI and FPI controllers, (b) Torque response of the PI and FPI controllers, (c) Stator current response in the *d*- and *q*-axis of the PI and FPI controllers, and (d) Three-phase current response of the PI and FPI controllers

4.2. Speed changes over time and operates in FW mode

In this simulation, the *d*-axis stator current becomes negative, allowing the system to maintain a specified speed. The control signal, defined by the function fcn(t), dictates that when t < 0.3 sec, the reference speed ω_{ref} increases linearly, and when $t \geq$ 0.3 sec, it is limited to 2000 rpm. Fig. 11 (a) shows that the PI controller experiences a significant overshoot around 0.3 sec, resulting in oscillations and a prolonged stabilization period. In contrast, the FPI controller reaches the reference speed smoothly and quickly, without overshoot or oscillations, indicating enhanced stability and responsiveness. The enlarged view emphasizes the FPI's strength, while Figs. 11 (b), (c), and (d) illustrate that the FPI maintains higher stability and faster torque control and load response compared to the PI controller.

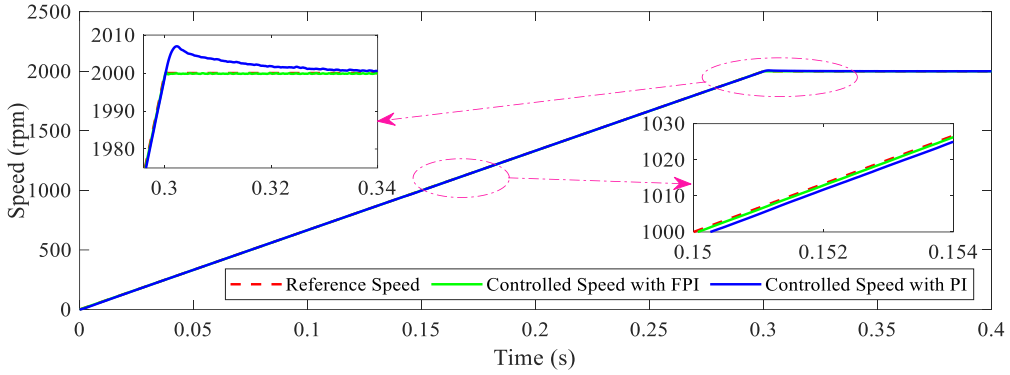

(a)

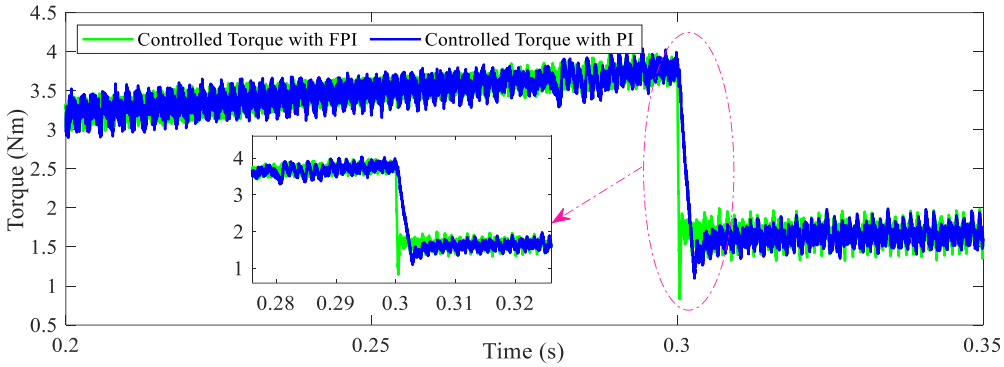

(b)

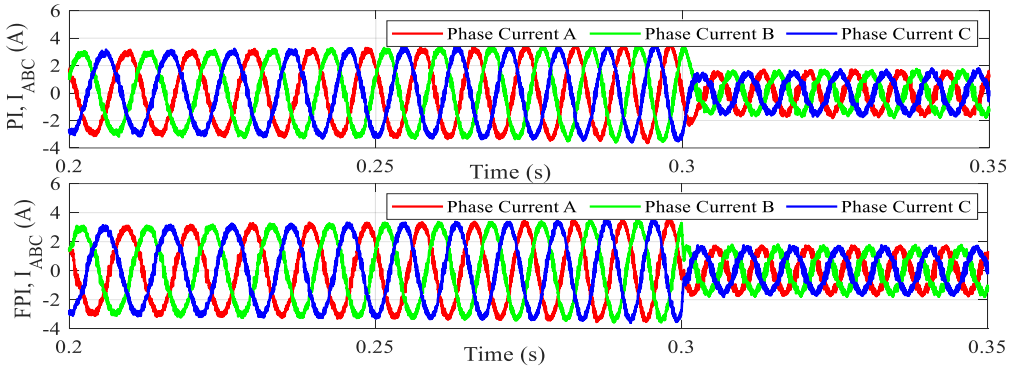

(c)

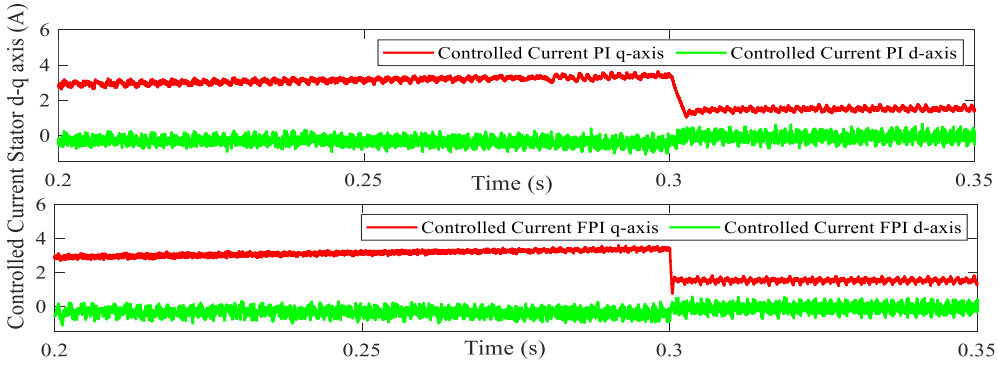

(d)

Figure. 11 PMSM control by MTPA-FW when set speed ω_{ref} = 2000 (rpm): (a) Speed response of the PI and FPI controllers, (b) Torque response of the PI and FPI controllers, (c) Stator current response in the *d*- and *q*-axis of the PI and FPI controllers, and (d) Three-phase current response of the PI and FPI controllers

4.3. Load Variation Over Time Considering Current Harmonic Distortion

Figs. 12 (a) and (b) show that when the engine operates in MTPA mode, with a load of 10 Nm applied at two different times of 0.1 sec and 0.3 sec, the response-ability of the FPI controller has a faster response time, overshoot is reduced. Processing time is significantly improved compared to traditional PI controllers.

To calculate the %THD, considering a current cycle at time 0.2 sec, when the speed changes from 1000 rpm to 1200 rpm, the calculation results are presented in Table 4. From Table 4, we can calculate the total %THD, which is higher for the PI method, with a value of 146.12% compared to 137.16% for the FPI method. This indicates that the PI method generates higher harmonic distortion, meaning the three-phase current quality is worse than FPI. The FPI method significantly reduces the %THD, particularly in phase B, where the %THD drops from 109.56% to 81.33%. This demonstrates that FPI improves the current quality by reducing harmonic distortion in the system.

Fig. 13 shows the speed response of the PI and FPI controllers when the motor operates in MTPA-FW mode. In the transient phase 0.19-0.22 sec, the FPI controller fluctuates less, indicating better response and stability than the PI controller. Both controllers achieve stable speeds in a steady state of 0.3-0.4 sec, but the FPI responds faster and with minimal fluctuation. Using FW, the motor reaches 2000 rpm, surpassing the rated 1200 rpm. When a 5 Nm load is added, initial fluctuations stabilize quickly. Adding another 10 Nm load at 0.35 sec confirms the FPI's superior stability and faster response. Considering one current cycle after 0.3 s during the speed change to consider the total %THD, the calculation results are presented in Table 5. From Table 5, the total %THD of the PI method is 709.03%, which is higher than the FPI method at 647.77%. This indicates that the PI method produces more significant harmonic distortion, resulting in lower three-phase current quality than FPI. The FPI method significantly reduces %THD, particularly in phase B, where %THD decreases from 1199.93% to 1022.95%. This demonstrates that FPI improves current quality and reduces harmonic distortion in the system. This result has significantly added to the harmonic lightning protection and stability of the PMSM motor drive system, which was not proposed in the study [34].

Table 4 Total phase current harmonic distortion when the motor operates in MTPA mode

Controller	Phase Current	Fundamental (50Hz)	%THD
PI	*A*	5.211	81.42
	B	7.859	109.56
	C	3.161	247.37
FPI	*A*	3.228	225.23
	B	7.355	81.33
	C	7.284	104.91

Table 5 Total phase current harmonic distortion when the motor operates in MTPA-FW mode

Controller	Phase Current	Fundamental (50Hz)	%THD
PI	*A*	2.034	478.48
	B	0.8644	1199.93
	C	2.131	448.67
FPI	*A*	1.145	506.64
	B	0.5964	1022.95
	C	1.368	413.72

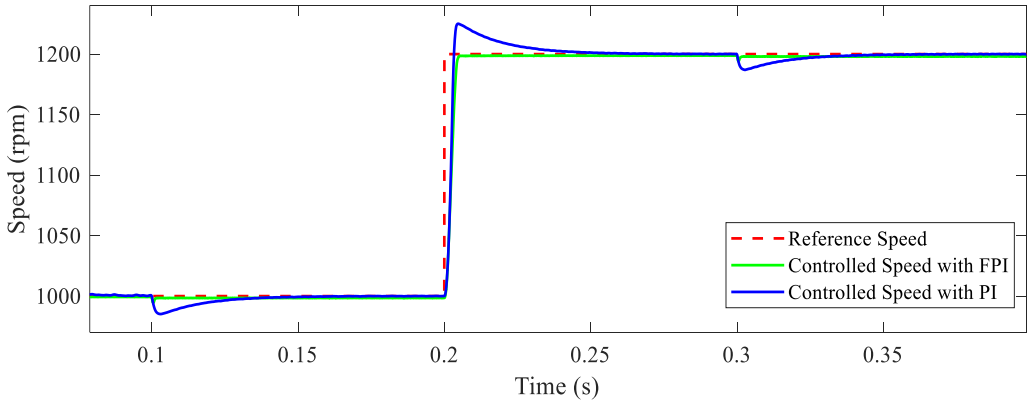

Figure. 12 Speed response of PMSM when applying load T_L = 10 (Nm) and operating in MTPA mode at the time of applying load 0.1 sec at the time of applying load 0.3 sec

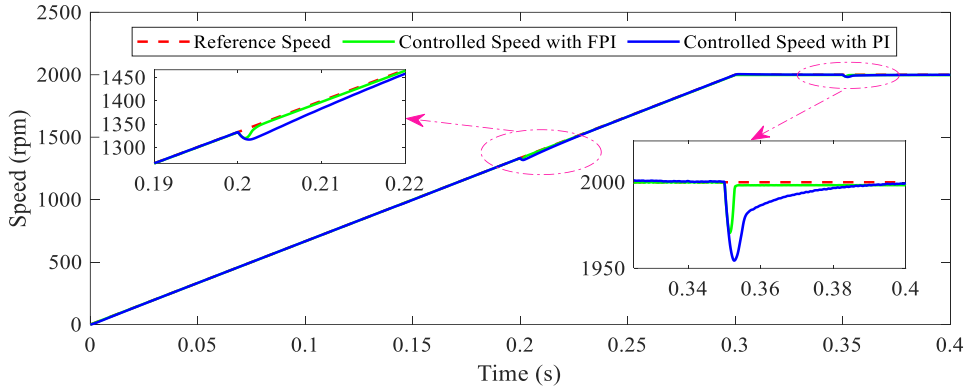

Figure. 13 Speed response of PMSM when applying load T_L= [5 10] (Nm) and operating in MTPA-FW mode, speed response at the time of load application 0.2 sec and Speed response at the time of load application 0.35 sec

Table 6. Torque values, copper losses, and efficiency for control methods

Method	Reference Speed (rpm)	*d*- and *q*-*axis* Current value (A)		Torque value (Nm)	Copper loss (W)	Efficiency (%)
		i_d	i_q			
Use the PI controller;	1000 ÷1200	0.05165	0.5393	0.5901	0.8436	98.88
Use the MTPA method with the PI controller;		-0.07317	0.5201	0.5717	0.7928	98.91
Use the MTPA method with the FPI controller;		-0.13780	0.3128	0.3446	0.3358	99.23
Use the MTPA-FW method with the PI controller;	2000	-0.05112	1.4930	1.6397	6.4138	96.98
Use the MTPA-FW method with the FPI controller.		0.01122	1.3640	1.4946	5.3474	97.23

Through three simulation cases, it can be concluded that the combination of MTPA-FW control and the FPI controller provides high accuracy and performs effectively with features such as stability under model parameter variations, load changes, and motor parameter adjustments. By integrating the three components, MTPA, FW, and FPI, this proposed method can achieve superior control performance, maximize efficiency, extend the operational range, and enhance the overall stability and responsiveness of the PMSM drive system. This makes it highly suitable for modern applications that demand high performance, energy efficiency, flexibility, and calculated loss values and efficiency, as provided in Table 6.

5. Conclusions

This study demonstrates the effectiveness of the proposed fuzzy logic-enhanced PI (FPI) controller combined with maximum torque per ampere (MTPA) and field weakening (FW) strategies in optimizing permanent magnet synchronous motor (PMSM) control. Significant performance differences between the controllers were evident through simulation results in MATLAB/Simulink. Simulation results reveal that the FPI controller outperforms traditional PI control in both MTPA and MTPA-FW modes. Specifically, it achieves an 8.96% reduction in THD in MTPA mode and a 61.26% reduction in MTPA-FW mode, along with improved motor efficiency by 0.35% and 0.26%, respectively. When switching to the MTPA-FW mode, the FPI controller demonstrates superior performance, significantly reducing %THD in the current phase I_B, with an average total reduction of 61.26%. This reduction in %THD improves current quality and positively impacts motor efficiency, speed stability, and energy loss reduction while minimizing thermal losses, extending component lifespan, and enhancing system stability. Specifically, the PI controller achieves an efficiency of 98.88% in MTPA mode, while the FPI controller increases this to 99.23%, a 0.35% improvement. In MTPA-FW mode, the PI controller achieves an efficiency of 96.98%, while the FPI controller improves it to 97.23%, a 0.26% increase. These enhancements lead to better current quality, reduced thermal losses, extended component lifespan, and greater system stability.

The study also highlights the potential of applying the FPI controller with MTPA-FW strategies in real-world systems, such as electric vehicles and autonomous aerial vehicles, where energy efficiency, speed stability, and precise control are crucial. The findings could enhance the efficiency and responsiveness of control systems in applications requiring high-speed and precise control. The findings underscore the practicality and reliability of this approach, offering a high-performance solution for PMSM applications in modern industries.

Conflicts of Interest

The authors declare no conflict of interest.

Author Contributions

Conceptualization, L.C.Q and C.N.D; methodology, H.H.B.N and L.V.D; software, L.V.D and C.N.D; validation, C.N.D, L.C.Q and H.H.B.N; formal analysis, L.C.Q and L.V.D; investigation, H.H.B.N; resources, C.N.D, L.V.D, and L.C.Q; data curation, C.N.D; writing original draft preparation, C.N.D and L.V.D; writing review and editing, H.H.B.N; visualization, L.C.Q, H.H.B.N and L.C.Q; supervision, H.H.B.N and L.V.D; project administration, L.V.D and H.H.B.N. All authors have read and agreed to the published version of the manuscript.

References

[1] Y. Wen, H. Zheng, F. Yang, and X. Zeng, "A novel MTPA and flux weakening method of stator flux oriented control of PMSM", *Transportation Safety and Environment*, Vol. 3, No. 3, p. tdab008, 2021.

[2] Y.-Z. Li, S.-J. Zhu, Y. Li, and Q. Lu, "Temperature prediction and thermal boundary simulation using hardware-in-loop method for permanent magnet synchronous motors", *IEEE/ASME Transactions on Mechatronics*, Vol. 21, No. 1, pp. 276-287, 2015.

[3] F. Niu, B. Wang, A. S. Babel, K. Li, and E. G. Strangas, "Comparative evaluation of direct torque control strategies for permanent magnet synchronous machines", *IEEE Transactions on Power Electronics*, Vol. 31, No. 2, pp. 1408-1424, 2015.

[4] X. Liu, H. Chen, J. Zhao, and A. Belahcen, "Research on the performances and parameters of interior PMSM used for electric vehicles", *IEEE Transactions on Industrial Electronics*, Vol. 63, No. 6, pp. 3533-3545, 2016.

[5] M. Pinilla and S. Martinez, "Selection of main design variables for low-speed permanent magnet machines devoted to renewable energy conversion", *IEEE Transactions on Energy Conversion*, Vol. 26, No. 3, pp. 940-945, 2011.

[6] T. Reichert, T. Nussbaumer, W. Gruber, and J. W. Kolar, "Bearingless permanent-magnet motor with 4/12 slot-pole ratio for bioreactor stirring applications", *IEEE/ASME Transactions on Mechatronics*, Vol. 16, No. 3, pp. 431-439, 2011.

[7] J. P. Desai, "Analytical Review of MTPA with Field Weakening Control of IPMSM on FEA Validated Design", *Transactions of the Indian National Academy of Engineering*, Vol. 8, No. 2, pp. 305-316, 2023.

[8] Q. D. Nguyen and S. Ueno, "Modeling and control of salient-pole permanent magnet axial-gap self-bearing motor", *IEEE/AsmE Transactions On Mechatronics*, Vol. 16, No. 3, pp. 518-526, 2010.

[9] M. Preindl and S. Bolognani, "Optimal state reference computation with constrained MTPA criterion for PM motor drives", *IEEE Transactions on Power Electronics*, Vol. 30, No. 8, pp. 4524-4535, 2014.

[10] Y. Nyanteh, C. Edrington, S. Srivastava, and D. Cartes, "Application of artificial intelligence to real-time fault detection in permanent-magnet synchronous machines", *IEEE transactions on industry applications*, Vol. 49, No. 3, pp. 1205-1214, 2013.

[11] T. Pajchrowski, K. Zawirski, and K. Nowopolski, "Neural speed controller trained online by means of modified RPROP algorithm", *IEEE transactions on industrial informatics*, Vol. 11, No. 2, pp. 560-568, 2014.

[12] A. Elhaj, M. Alzayed, and H. Chaoui, "MTPA Speed Control for IPMSM Drives Without Current Sensing", *IEEE Access,* 2024.

[13] M. Nicola, C. I. Nicola, D. Selișteanu, C. Ionete, and D. Șendrescu, "Improved Performance of the PMSM Sensorless Control System Based on DTC Strategy and SMC Using Fractional Order and Fractal Dimension Calculus", *Appl. Sci.*, Vol. 14, No. 19, 2024.

[14] M. U. Sardar, M. Yaqoob, S. Akbar, S. I. A. Shah, M. U. Shahid, and T. Mutloob, "Permanent Magnet Synchronous Machine Control Performance and Analysis for Environment-Friendly Electric Vehicle Applications", *Engineering Proceedings,* Vol. 46, No. 1, p. 7, 2023.

[15] D. Citharthan, M. Varatharaj, M. A. Babu, and S. Kannan, "Field oriented control of permanent magnet synchronous motor with dq axis

decoupling using feed forward compensation", In: *AIP Conference Proceedings*, Vol. 2831, No. 1, AIP Publishing, 2023.

[16] T. Sun, J. Wang, and X. Chen, "Maximum torque per ampere (MTPA) control for interior permanent magnet synchronous machine drives based on virtual signal injection", *IEEE Transactions on Power Electronics*, Vol. 30, No. 9, pp. 5036-5045, 2014.

[17] Y. Alsayed, A. Maamoun, and A. Shaltout, "High performance control of PMSM drive system implementation based on DSP real-time controller", In: *Proc. of* in *2019 International Conference on Innovative Trends in Computer Engineering (ITCE)*, : IEEE, pp. 225-230, 2019.

[18] A. Maamoun, Y. Alsayed, and A. Shaltout, "Fuzzy logic based speed controller for permanent-magnet synchronous motor drive", In: *Proc. of* in *2013 IEEE International Conference on Mechatronics and Automation*, pp. 1518-1522, : IEEE, 2013.

[19] I. Qureshi and V. Sharma, "Wide speed range and torque control of ipmsm with mtpa-mtpv field weakening control", *Arabian Journal for Science and Engineering,* pp. 1-16, 2023.

[20] I. Qureshi and V. Sharma, "PMSM motor drive and their control schemes", *Journal of Applied Research and Technology,* Vol. 22, No. 2, pp. 274-283, 04/30 2024, doi: 10.22201/icat.24486736e.2024.22.2.2321.

[21] Z. Mynar, L. Vesely, and P. Vaclavek, "PMSM model predictive control with field-weakening implementation", *IEEE Transactions on Industrial Electronics,* Vol. 63, No. 8, pp. 5156-5166, 2016.

[22] V. T. Ha and P. T. Giang, "Field—weakening control with maximum torque per ampere (mtpa) for electric vehicle (ev) application", In: *Proc. of* in *International Conference on Green Technology and Sustainable Development*, pp. 531-541, 2022.

[23] K. Lu and Z. Q. Zhu, "Comparative Stability Analysis of IPMSM and SPMSM Machines Under Flux-Weakening Control", In: *Proc. of 2024 International Conference on Electrical Machines (ICEM)*, pp. 1-7, 2024.

[24] H. Zaimen, A. Rezig, and S. Touati, "Open-Switch Fault Tolerance Strategy for Induction Motor Drive System", *Journal of Operation and Automation in Power Engineering,* 2024.

[25] S. Ferdous, P. Garcia, M. A. M. Oninda, and M. A. Hoque, "MTPA and field weakening control of synchronous reluctance motor", In: *Proc. of* in *2016 9th International Conference on Electrical and Computer Engineering (ICECE)*, pp. 598-601, 2016.

[26] J. Balda, "Permanent magnet synchronous motor drive for HEV propulsion: Optimum speed ratio and parameter determination", In: *Proc. of IEEE 56th Vehicular Technology Conference*, Vol. 3, pp. 1500-1504, 2002.

[27] M. Nicola, C.-I. Nicola, D. Selișteanu, and C. Ionete, "Control of PMSM based on switched systems and field-oriented control strategy", *Automation,* Vol. 3, No. 4, pp. 646-673, 2022.

[28] N. D. Hung, "Voltage Stability Improvement of Synchronous Generator by Using AVR Self Turning Based on the Adaptive Fuzzy-PID Controller", *International Journal of Intelligent Engineering & Systems,* Vol. 15, No. 6, 2022, doi: 10.22266/ijies2022.1231.42.

[29] J. Yu, J. Gao, Y. Ma, H. Yu, and S. Pan, "Robust adaptive fuzzy control of chaos in the permanent magnet synchronous motor", *Discrete Dynamics in Nature and Society,* Vol. 2010, No. 1, p. 269283, 2010.

[30] Y. Zhang, Y. Liang, and Y. Dong, "Research on Field Weakening Control of PMSM Based on Improved Single Current Regulator", In: *Proc. of 2022 34th Chinese Control and Decision Conference (CCDC)*, pp. 3718-3723, 2022.

[31] N. Vu Quynh, "The fuzzy PI controller for PMSM's speed to track the standard model", *Mathematical Problems in Engineering,* Vol. 2020, No. 1, p. 1698213, 2020.

[32] K. Bai and K.-M. Lee, "Direct field-feedback control of a ball-joint-like permanent-magnet spherical motor", *IEEE/ASME Transactions on Mechatronics,* Vol. 19, No. 3, pp. 975-986, 2013.

[33] F. Aghili, "Energy-efficient and fault-tolerant control of multiphase nonsinusoidal pm synchronous machines", *IEEE/ASME Transactions on Mechatronics,* Vol. 20, No. 6, pp. 2736-2751, 2015.

[34] E. G. Shehata, Y. S Mohamad, and A. A. Z. Diab, "High performnace control of permanent magnet synchronous motor under different modes of operation", *Journal of Advanced Engineering Trends,* Vol. 42, No. 2, pp. 245-255, 2023.